Open access • Journal Article • DOI:10.1016/S0082-0784(98)80505-5

Ignition of hydrogen-air mixing layer in turbulent flows — Source link

Hong G. Im, J. H. Chen, Chung K. Law

Institutions: Sandia National Laboratories, Princeton University

Published on: 01 Jan 1998

Topics: Minimum ignition energy, Ignition system, Turbulence kinetic energy, Direct numerical simulation and Turbulence

Ignition of Hydrogen/Air Mixing Layer in Turbulent Flows*

H. G. IM and J. H. CHEN
Combustion Research Facility
Sandia National Laboratories, Livermore, CA 94551

C. K. LAW
Department of Mechanical and Aerospace Engineering
Princeton University, Princeton, NJ 08544

Corresponding author:
Dr. Hong G. Im
Combustion Research Facility, MS 9051
Sandia National Laboratories
Livermore, CA 94551-0969, USA

Phone: (510) 294-3131
Fax: (510) 294-2595
email: hgim@ca.sandia.gov

Word Count:
Text: 2850 (estimate 300 words/page × 9.5 pages)
Tables: 100
Figures: 2600 (13 × 200)
Total: 5550

Preferred Presentation:
Oral

Preferred colloquium topic area:
Turbulent Non-Premixed Combustion (Ignition)

*Submitted to the 27th Symposium (International) on Combustion, Boulder, CO, August 2-7, 1998.

DISCLAIMER

Abstract

Autoignition of a scalar hydrogen/air mixing layer in homogeneous turbulence is studied using direct numerical simulation. An initial counterflow of unmixed nitrogen-diluted hydrogen and heated air is perturbed by two-dimensional homogeneous turbulence. The temperature of the heated air stream is chosen to be 1100K which is substantially higher than the crossover temperature at which the rates of the chain branching and termination reactions become equal. Three different turbulence intensities are tested in order to assess the effect of the characteristic flow time on the ignition delay. For each condition, a simulation without heat release is also performed. The ignition delay determined with and without heat release is shown to be almost identical up to the point of ignition for all of the turbulence intensities tested, and the predicted ignition delays agree well within a consistent error band. It is also observed that the ignition kernel always occurs where hydrogen is focused, and the peak concentration of HO_2 is aligned well with the scalar dissipation rate. The dependence of the ignition delay on turbulence intensity is found to be nonmonotonic. For weak to moderate turbulence the ignition is facilitated by turbulence via enhanced mixing, while for stronger turbulence, whose timescale is substantially smaller than the ignition delay, the ignition is retarded due to excessive scalar dissipation, and hence diffusive loss, at the ignition location. However, for the wide range of initial turbulence fields studied, the variation in ignition delay due to the corresponding variation in turbulence intensity appears to be quite small.

Introduction

Understanding autoignition in a hydrogen/air system is of importance not only for the utilization of hydrogen as a fuel, but also because hydrogen chemistry is a building block for more complex chemistry involving hydrocarbon fuels. While some basic chemical behavior of various pressure/temperature regimes has long been known for a homogeneous explosion system [1], recent studies of the ignition of hydrogen/air within a convective/diffusive environment have revealed many additional interesting characteristics of such a system[2-8]. In particular, the studies of hydrogen against heated air in a counterflow [3] and laminar mixing layer [7] have identified chemical behavior leading to ignition in various temperature/pressure regimes, which was further substantiated by a bifurcation analysis [8]. One of the key findings of these studies is that, for ignition temperatures higher than the crossover temperature, at which the rates of branching and three-body termination reactions of H and O_2 become equal, ignition can be described purely by a chemical nonlinear coupling without having to involve thermal feedback. The importance of the chain-branching reaction, H + HO_2 = OH + OH, during the chemical runaway was first identified by Kreutz and Law [3]. This result suggests a significant simplification in identifying ignition events in more complex practical combustion systems by alleviating numerical difficulties related to heat release.

In many combustion devices, autoignition is achieved by injecting a relatively cold combustible into hot air. Therefore, the chemical development and turbulent mixing are strongly coupled, and both are important processes during the induction period. Since ignition is a local event, it can be generally anticipated that turbulence will most likely facilitate the production of well-mixed ignition kernels such that ignition is promoted compared to the situation with pure laminar mixing. A recent study by Mastorakos *et al.* [9] confirmed this

result from numerical simulation of ignition in a turbulent mixing layer with simplified chemistry, for relatively weak turbulence intensities.

In the present study we perform DNS of ignition in a two-dimensional turbulent mixing layer of hydrogen and heated air using detailed chemistry, thereby providing a more complete realization of the ignition event. A wide range of turbulence intensities is covered in order to assess the effect of turbulence intensity on the ignition delay. The spatial distribution of various species and scalar dissipation rates is also analyzed. Finally, the issue of chemical runaway in characterizing the ignition event and the behavior of the associated key reaction steps in turbulent flows are examined by comparing results with and without heat release for each of the turbulent flows.

Numerical Solution

The full compressible Navier-Stokes, species and energy equations for a reacting gas mixture are solved using a fourth-order Runge-Kutta method for time integration and an eighth-order explicit spatial differencing scheme [10]. We adopt the chemical mechanism developed by Yetter *et al.* [11] with 9 species and 38 reversible reactions, which has been shown to capture the ignition process successfully. The molecular viscosity is temperature dependent ($\sim T^{0.7}$) and the Prandtl number is taken to be 0.708. The mass diffusion coefficients for individual species are determined by constant Lewis numbers given as

$$Le_{H_2} = 0.3,\ Le_{O_2} = 1.11,\ Le_{O} = 0.7,\ Le_{OH} = 0.73,$$

$$Le_{H_2O} = 0.83,\ Le_{H} = 0.18,\ Le_{HO_2} = 1.10,\ Le_{H_2O_2} = 1.12.$$

The spatial and temporal variables for the compressible reacting flow are nondimensionalized by acoustic scales which take the value of $L_{ref} = 4.50$ mm and $\tau_{ref} = 1.29 \times 10^{-5}$ sec. The

computational domain is a two-dimensional square of size L_{ref}, for which 501×501 grid resolution is used. For all calculations, the initial pressure was uniformly taken to be 1 atm. Boundary conditions are nonreflecting in the direction of the initial mixture fraction gradient and periodic in the direction perpendicular to it.

Figure 1 shows a schematic of the problem configuration. For the initial condition, a mixing layer of thickness δ separates diluted hydrogen and heated air on each side. The mixing layer profile is given as

$$Y_{H_2} = Y_{H_2,0} f(x), \quad Y_{O_2} = Y_{O_2,L}[1 - f(x)], \quad T = T_0 + (T_L - T_0) f(x), \tag{1}$$

where $f(x) = 0.5[1 - \mathrm{erf}\{4(x - x_m)/\delta\}]$ has a characteristic thickness δ centered at $x = x_m$. We choose the value $\delta/L_{ref} = 0.02$ in this study. The fuel side is diluted with nitrogen by 50% volume such that $Y_{H_2,0} = 0.0667$ at $T_0 = 300$K, and $Y_{O_2,L} = 0.233$ at $T_L = 1100$K on the heated air side. The turbulence is prescribed by an initial two-dimensional turbulent kinetic energy spectrum function [12] which is superimposed on the initial field with zero velocity. To examine the issue of chemical runaway, each case has been run with and without the heat release terms in the energy equation, and the results are compared in terms of predicted ignition delays.

Results and Discussion

Ignition in a One-dimensional Laminar Flow

As a point of reference, we first examine a one-dimensional laminar ignition problem for the same initial condition as in Eq. (1). Figure 2 shows the time evolution of temperature and species profiles during ignition. Here we choose the elemental mixture fraction for H, ξ_H [13], as the independent variable. It is seen that the peak concentrations of radicals increase

enormously, by many orders of magnitude, before the temperature field shows any noticeable peak due to reaction. It is also noted that, while the stoichiometric mixture fraction, $\xi_{H,st}$, is 0.304 for this condition, during ignition the maximum radical concentrations are located further into the heated air side at approximately $\xi_H = 0.1 \sim 0.15$, which we define as the *ignition kernel*, as observed in previous studies [2, 9].

The evolution of the maximum temperature and species concentrations is plotted as a function of time, both with and without heat release, in Fig. 3. It is seen that the two results for radical concentrations are identical almost up to the ignition point, during which the value rises by several orders of magnitude. We define ignition delay as the time at which the marker variable, typically H, reaches a maximum temporal gradient. In this case, the ignition delays based on H radical with and without heat release are respectively 0.137 and 0.126 milliseconds, with a difference of approximately 8%. This confirms the dominance of chemical nonlinearity during ignition, consistent with the results of recent studies [2, 7].

In Fig. 3, we note two distinct features in the evolution of HO_2 radical. First, HO_2 rises very rapidly in the beginning, then slows down as the ignition point is approached while other major radicals, such as H, O and OH, continue to increase exponentially. Furthermore, we observe that maximum HO_2 concentrations with and without heat release remain remarkably close even beyond the ignition point. To understand this distinct behavior, we first note that the main production of HO_2 is through the reaction

$$H + O_2 + M = HO_2 + M, \tag{R9}$$

which competes with the branching reaction

$$H + O_2 = O + OH. \tag{R1}$$

Furthermore, previous studies [3, 8] have demonstrated that an additional branching path

$$HO_2 + H = OH + OH \tag{R11}$$

becomes increasingly important as the ignition point is approached. A secondary path for HO_2 consumption also occurs through the reaction

$$HO_2 + H = H_2 + O_2. \tag{R10}$$

Figure 4 shows the evolution of temperature and HO_2 mass fraction profiles. It is seen that the peak concentration starts to occur in the vicinity of the ignition kernel, *i.e.* at approximately $\xi_H = 0.15$, but as ignition progresses the peak point moves toward the colder fuel side. Thus, the location of peak HO_2 remains at lower temperatures even beyond the ignition point, resulting in no noticeable difference from the peak value without heat release. At $t/\tau_{ref} = 12$, it is noted that another peak of HO_2 begins to develop at the edge of the oxidizer side of the flame. We observe that this new peak is the actual location of maximum HO_2 for the diffusion flame, for which the earlier larger peak completely disappears. Figure 5 further shows the details of the reaction balance at two representative stages in time. At an earlier stage ($t/\tau_{ref} = 5$), the production of HO_2 is dominated by R9, while the contributions of both R11 and R10 are negligible. As the radical pool develops near the ignition point ($t/\tau_{ref} = 10$), however, the consumption by R11 and R10 almost balances with production by R9, and the net reaction rate exhibits a much smaller peak further into the fuel stream. This further substantiates the importance of the branching step R11 in radical runaway, as found in previous studies [3, 7, 8].

Ignition in Two-dimensional Turbulent Flows

We now investigate the ignition behavior in two-dimensional turbulent flows. The turbulent flow field is characterized by an integral length scale, L_{11}, and time scale $\tau_{turb} = k^{3/2}/\epsilon$, where k and ϵ are, respectively, the turbulent kinetic energy and dissipation rate. In this study we use three different turbulent flow fields characterized by the following initial conditions:

- Weak turbulence: $L_{11}/\delta = 10.1$, $\tau_{turb}/\tau_{ref} = 29.2$,
- Moderate turbulence: $L_{11}/\delta = 5.9$, $\tau_{turb}/\tau_{ref} = 8.6$,
- Strong turbulence: $L_{11}/\delta = 3.8$, $\tau_{turb}/\tau_{ref} = 2.8$.

In the ignition problem, the characteristic time scales of turbulence relative to the ignition delay are of physical importance. Since the ignition delay of the one-dimensional laminar case, shown in Fig. 3, is approximately $\tau_{ig}/\tau_{ref} = 10$, the three cases represent $\tau_{turb}/\tau_{ig} \approx 3$, 1 and 0.3, respectively.

Figures 6 and 7 show the contours of H at an earlier stage ($t/\tau_{ref} = 5$) and near ignition ($t/\tau_{ref} = 10$) for the weak and strong turbulence cases, respectively. Overlaid in the figures are the contours of the scalar dissipation rate defined as $\chi_H = 2\alpha|\nabla\xi_H|^2$, where $\alpha = \lambda/\rho c_p$ is the local thermal diffusivity. We first note that, regardless of the strength of the turbulence, the ignition kernel tends to be located around the mixing layer which is *convex* to the fuel side. Although not shown here, the contours for the moderate turbulence case also reveal the same behavior. This is expected considering the focusing of highly-diffusive hydrogen at such locations where oxygen is abundant at higher temperatures.

Comparing Figs. 6 and 7, it is also seen that, while for weak turbulence there is a single dominant ignition kernel throughout the whole induction period, for strong turbulence several

ignition kernels with comparable reaction strength evolve simultaneously, with the location for the maximum concentration shifting in time. For the turbulence fields considered in this study, we find that this "shift" occurs once and twice for the moderate and strong turbulence cases, respectively, during the entire induction period. It is expected that, as the turbulence intensity becomes higher, the local scalar dissipation rate at the ignition kernel fluctuates more rapidly, such that it is less likely to sustain an *optimal* ignition condition (*i.e.* the minimum dissipation rate) at a single location throughout the entire induction period. Consequently, the maximum ignition kernel will likely change from one location to the next.

Figures 8 and 9 show the maximum temperature and several intermediate species mass fractions as a function of time for the weak and strong turbulence cases, respectively. For a fairly wide range of relative turbulence intensity, it appears that the overall physico-chemical mechanism during ignition remains the same. As in the reference case (Fig. 3), the appearance of the the radical runaway before a substantial temperature rise is clearly seen in both Figs. 8 and 9, such that the result without heat release (dotted curves) shows almost no difference all the way up to the ignition point. To substantiate this matter, the ignition delays based on H, as defined in the previous section, for the various cases are reported in Table 1. It is seen that, for all cases studied, not only are the relative differences small, but the relative magnitude among the four cases is also consistent with that with heat release, confirming the validity of the radical-ignition concept.

The reaction flux analysis for the turbulent ignition shows the same behavior for the reaction rate of HO_2, as described in Fig. 5. The earlier decline in the rate of increase in HO_2 in Figs. 8 and 9 is consistent with the one-dimensional result. Consequently, as ignition is approached, an excessive amount HO_2 is accumulated near the location at the highest

dissipation rate. Figure 10 shows that, during the major evolution period of ignition, the HO_2 concentration aligns with the maximum scalar dissipation rate, thereby serving as a good marker species both for turbulence fields and for ignition.

Considering the wide range of turbulence fields studied, over which τ_{turb} changes by an order of magnitude, the variations in the ignition delay shown in Table 1 appear to be surprisingly small. This is consistent with the previous study [9] which concluded that, since ignition is a local phenomenon, any strength of turbulent flow will produce a few sufficiently *well-mixed* spots that will become the ignition kernel. It should also be taken into account that the turbulence is decaying in time in the present DNS simulations. Our estimates show that, for the strong turbulence case, the turbulent kinetic energy, k, decreases to 0.4 times, or τ_{turb} increases to 2.3 times, the initial value during the induction period.

Nevertheless, for the particular cases studied here, we cautiously note the nonmonotonic behavior in the ignition delay shown in Table 1, *i.e.* the strong turbulence case leading to a slightly longer ignition delay compared to the other cases. To identify the reason for this, in Fig. 11 we plot the reaction rate of H versus the scalar dissipation rate, conditioned over the range, $0.5 < \xi_H < 0.15$, in order to isolate the intensively reacting regions. The solid curve denotes the reference one-dimensional case. It is seen that, as the turbulence intensity increases, there is wider scatter from the laminar result. In particular, for the strong turbulence case, denoted by the red symbols, the overall reaction rate is suppressed compared to the weaker turbulence cases at the same χ_H. Furthermore, the maximum reaction rate is shifted further into the higher χ_H side, which is responsible for the longer ignition delay. Knowing the location at which the final ignition is achieved, we also monitor the history of the local scalar dissipation rate at this ignition kernel, as shown in Fig. 12.

It is seen that the ignition kernels for the weak and moderate turbulence cases experience slightly lower, yet comparable dissipation rates throughout the entire induction period. For the strong turbulence case, the local dissipation rate is initially much higher than the other cases, subsequently showing a more rapid variation in time. The large dissipation rate in the earlier stage is partly responsible for the longer ignition delay for the strong turbulence case. Therefore, it may be conjectured that, for strong turbulence with $\tau_{turb} < \tau_{ig}$, it is less likely to sustain low dissipation rate at a particular ignition kernel throughout the entire induction period, and thus a longer delay compared to moderate turbulence can be expected. Considering the random nature of turbulence, however, more statistical samples are needed to resolve this issue.

Conclusions

Ignition of hydrogen/air mixing layer in homogeneous decaying turbulence is studied where the range of turbulence time scales relative to the ignition delay is varied by an order of magnitude. For the same flows, parallel simulations with heat release suppressed were also performed. The results demonstrate that the solutions with and without heat release are almost identical up to the point of ignition for all of the turbulence fields considered, and the predicted ignition delays agree well within a consistent error band. The results imply that ignition of hydrogen/air in turbulent flow fields can also be characterized purely by *radical* runaway as opposed to thermal runaway, and as such, also holds the potential of alleviating numerical difficulties related to abrupt heat release, as suggested in a previous study [14].

We have also confirmed the role of the branching reaction, $HO_2 + H = OH + OH$, for chemical ignition. As the ignition point is approached, the branching reaction becomes increasingly important such that the peak HO_2 concentration is shifted further towards the

cold fuel stream, which eventually vanishes at the intensive burning state. Consequently, it was shown that the HO_2 peaks align with the maximum scalar dissipation rate during the ignition process. It was also observed that the ignition kernel tends to be located where the mixing layer is convex toward the fuel side due to the high diffusivity of the hydrogen molecules.

As for the effect of the turbulence-chemistry interaction, for the wide range of initial turbulence fields studied, the ignition delays appear to be quite insensitive to the turbulence intensity. It may be stated that, as ignition is a local event, there will always be some well-mixed regions as long as some turbulence exists. For stronger turbulence, whose timescale is smaller than the ignition delay, it was observed that ignition is slightly retarded due to the large magnitude of the scalar dissipation rate and its fluctuations at the ignition location. More data are needed to conclusively address this issue.

Acknowledgment

HGI and JHC were supported by the United States Department of Energy, Office of Basic Energy Sciences, Chemical Sciences Division, while CKL was supported by the Army Research Office. The authors would like to thank Dr. T. Echekki of Sandia National Laboratories for helpful comments.

References

[1] Lewis, B. and von Elbe, G., *Combustion, Flames and Explosions of Gases*, 3rd ed., Academic Press, 1987, p. 25.

[2] Kreutz, T. G., Nishioka, M. and Law, C. K., *Combust. Flame*, 99:758-766 (1994).

[3] Kreutz, T. G. and Law, C. K., *Combust. Flame*, 104:157-175 (1996).

[4] Balakrishnan, G., Smooke, M. D. and Williams, F. A., *Combust. Flame*, 102:329-340 (1995).

[5] Sánchez, A. L., Liñán, A. and Williams, F. A., *Twenty-Fifth Symposium (Internation) on Combustion*, The Combustion Institute, Pittsburg, PA, 1994, pp. 1529-1537.

[6] Treviño, C. and Liñán, A., *Combust. Flame*, 103:129-141 (1995).

[7] Nishioka, M. and Law, C. K., *Combust. Flame*, 108:199-219 (1997).

[8] Helenbrook, B. T., Im, H. G. and Law, C. K., *Combust. Flame*, 112:242-252 (1998).

[9] Mastorakos, E., Baritaud, T. A. and Poinsot, T. J., *Combust. Flame*, 109:198-223 (1997).

[10] Kennedy, C. A. and Carpenter, M. H., *Appl. Num. Math.*, 14:297-443 (1996).

[11] Yetter, R. A., Dryer, F. L. and Rabitz, H., *Combust. Sci. Tech.*, 79:97-128 (1991).

[12] Baum, M., Poinsot, T. J., Haworth, D. C. and Darabiha, N., *J. Fluid Mech.*, 281:1-32 (1994).

[13] Warnatz, J., Maas, U. and Dibble, R. W., *Combustion*, Springer-Verlag, 1995, p. 127.

[14] Sung, C. J. and Law, C. K., *Combust. Sci. Tech.*, in press (1998).

	W/ heat rel.	W/O heat rel.	Error
1-D laminar	0.1374	0.1260	0.083
Weak turbulence	0.1293	0.1208	0.066
Moderate turbulence	0.1301	0.1219	0.063
Strong turbulence	0.1385	0.1301	0.061

Table 1 Ignition delay based on maximum temporal gradient of Y_H for various cases. Units are in milliseconds.

Figure Captions

Figure 1 Schematic of the problem configuration.

Figure 2 Evolution of temperature (dotted) and Y_{H} profiles (solid) during the ignition event for one-dimensional problem; ····· : $t/\tau_{ref} = 5$; ---- : $t/\tau_{ref} = 7$; —·— : $t/\tau_{ref} = 9$; —— : $t/\tau_{ref} = 10$. Note that the temperature profiles at $t/\tau_{ref} = 5$ and 7 are indistinguishable.

Figure 3 Maximum temperature and species as a function of time for the one-dimensional problem; bold line denotes with heat release and thin line denotes without heat release. The vertical dashed line indicates the ignition time based on the maximum temporal gradient of Y_H for the case with heat release.

Figure 4 Temperature (dotted) and $Y_{\mathrm{HO_2}}$ profiles (solid) during the ignition event for the one-dimensional problem; ····· : $t/\tau_{ref} = 5$; ---- : $t/\tau_{ref} = 8$; —·— : $t/\tau_{ref} = 10$; —— : $t/\tau_{ref} = 12$. The temperature profiles at $t/\tau_{ref} = 5$ and 7 are indistinguishable. Note that $Y_{\mathrm{HO_2}}$ at t/τ_{ref} is magnified by 100 times.

Figure 5 Contributions of individual elementary reaction steps to the net reaction rate of HO_2 for (a) $t/\tau_{ref} = 5$ and (b) $t/\tau_{ref} = 10$.

Figure 6 Contours of Y_{H} (color) and χ_{H} (line) at an earlier stage ($t/\tau_{ref} = 5$) and near ignition ($t/\tau_{ref} = 10$) for the weak turbulence case.

Figure 7 Contours of Y_{H} (color) and χ_{H} (line) at an earlier stage ($t/\tau_{ref} = 5$) and near ignition ($t/\tau_{ref} = 10$) for the strong turbulence case.

Figure 8 Maximum temperature and species as a function of time for weak turbulence case, $\tau_{turb}/\tau_{ig} = 3$; bold line is with heat release and thin line without heat release.

Figure 9 Maximum temperature and species as a function of time for strong turbulence case, $\tau_{turb}/\tau_{ig} = 0.3$; bold line denotes with heat release and thin line denotes without heat release.

Figure 10 Contours of Y_{HO_2} (color) and χ_H (line) at an earlier stage ($t/\tau_{ref} = 5$) and near ignition ($t/\tau_{ref} = 10$) for the strong turbulence case.

Figure 11 Scatter plot for the reaction rate of H as a function of scalar dissipation rate for three turbulence cases at $t/\tau_{ref} = 3$. Solid curve denotes the one-dimensional laminar result. The turbulent data are conditioned around $0.05 < \xi_H < 0.15$ for which maximum reaction rate is obtained.

Figure 12 History of local scalar dissipation rate at the ignition kernel at which ignition finally occurs.

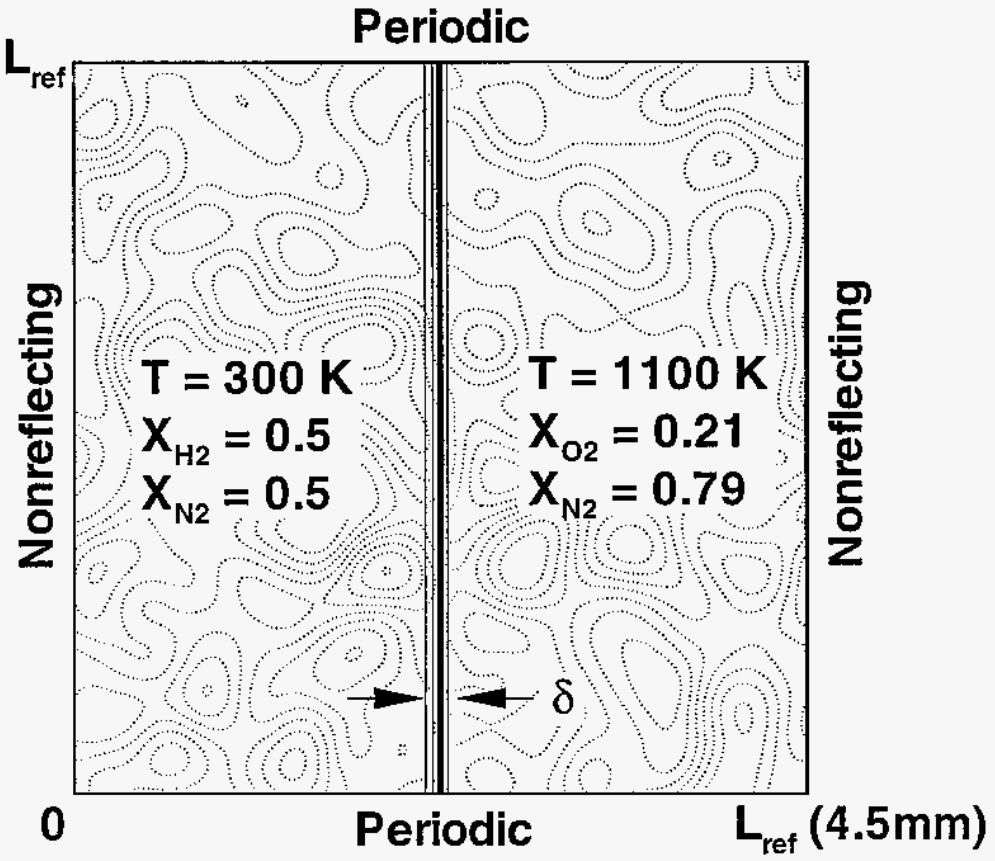

Figure 1: Schematic of the problem configuration.

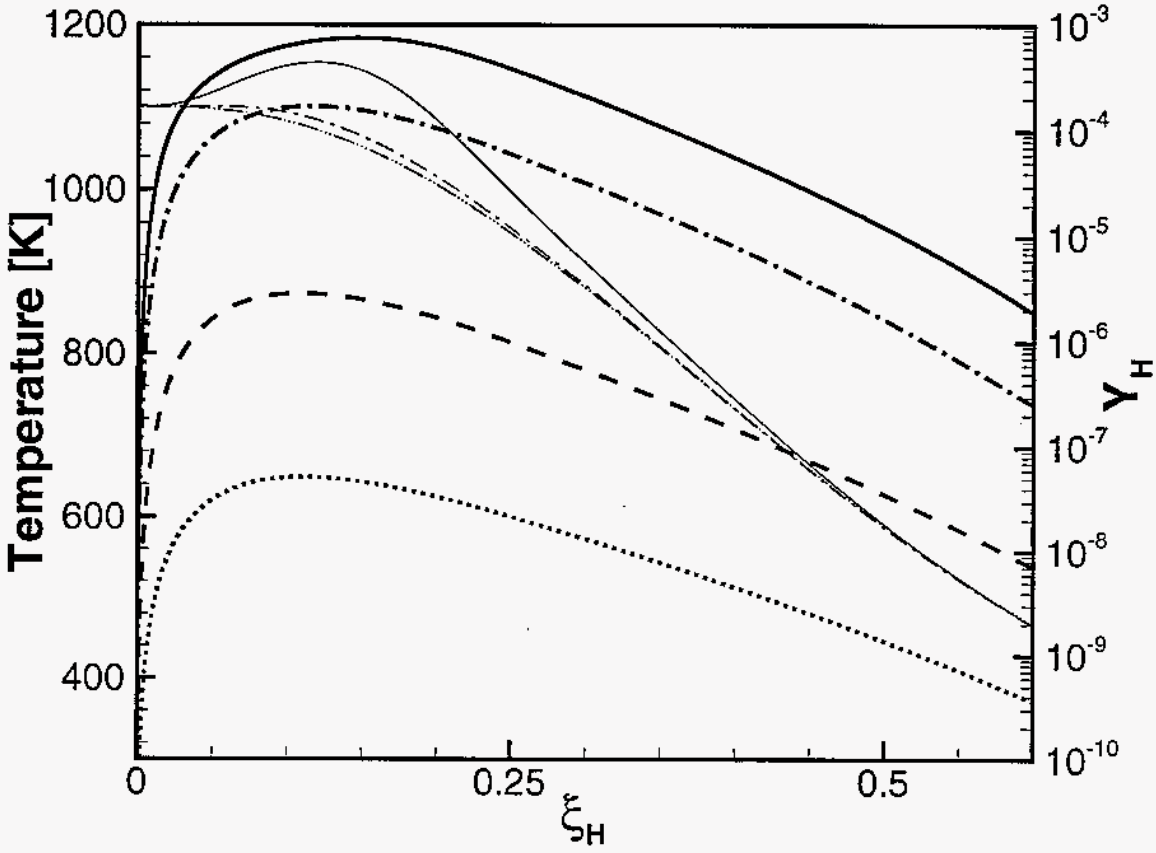

Figure 2: Evolution of temperature (dotted) and Y_H profiles (solid) during the ignition event for one-dimensional problem; ····· : $t/\tau_{ref} = 5$; ---- : $t/\tau_{ref} = 7$; —·— : $t/\tau_{ref} = 9$; —— : $t/\tau_{ref} = 10$. Note that the temperature profiles at $t/\tau_{ref} = 5$ and 7 are indistinguishable.

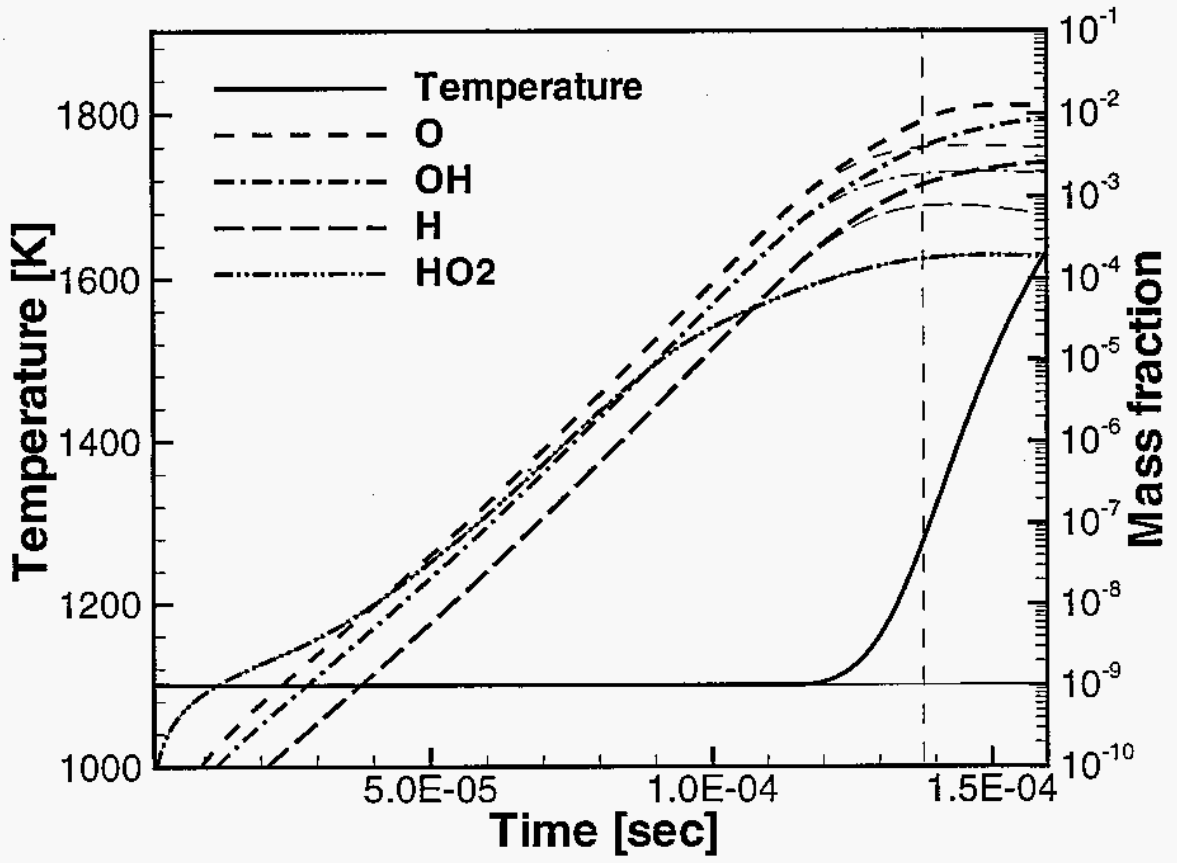

Figure 3: Maximum temperature and species as a function of time for the one-dimensional problem; bold line denotes with heat release and thin line denotes without heat release. The vertical dashed line indicates the ignition time based on the maximum temporal gradient of Y_H for the case with heat release.

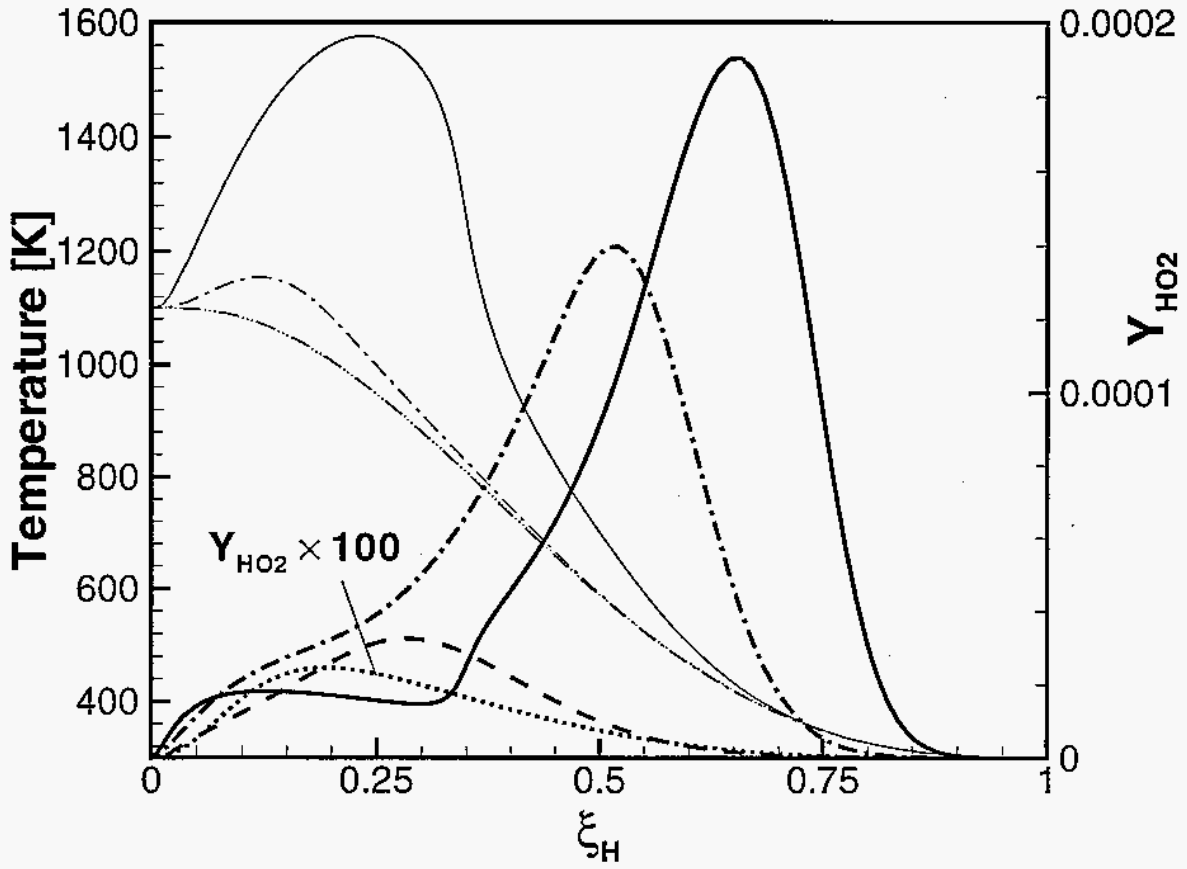

Figure 4: Temperature (dotted) and Y_{HO_2} profiles (solid) during the ignition event for the one-dimensional problem; ····· : $t/\tau_{ref} = 5$; ---- : $t/\tau_{ref} = 8$; —·— : $t/\tau_{ref} = 10$; —— : $t/\tau_{ref} = 12$. The temperature profiles at $t/\tau_{ref} = 5$ and 7 are indistinguishable. Note that Y_{HO_2} at t/τ_{ref} is magnified by 100 times.

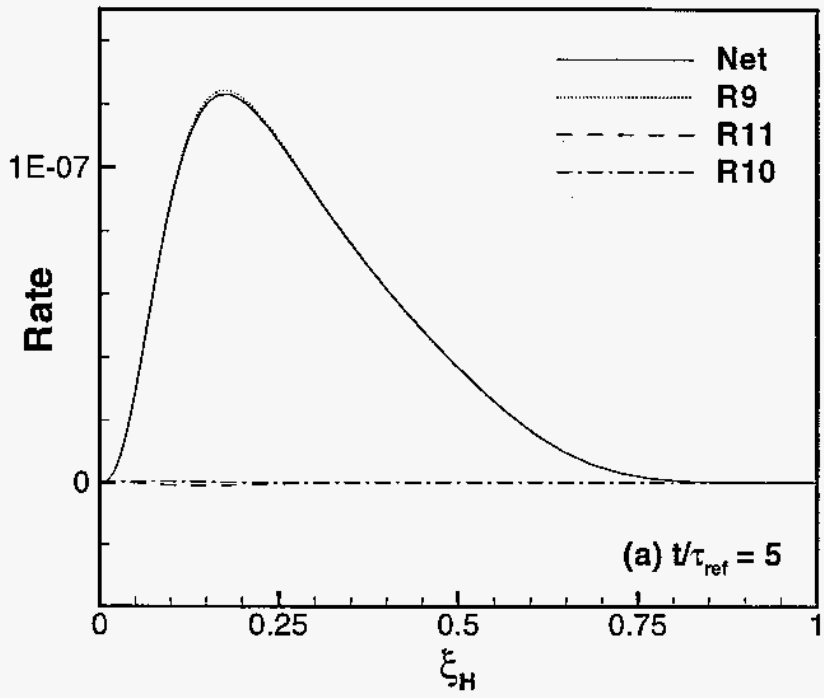

(a)

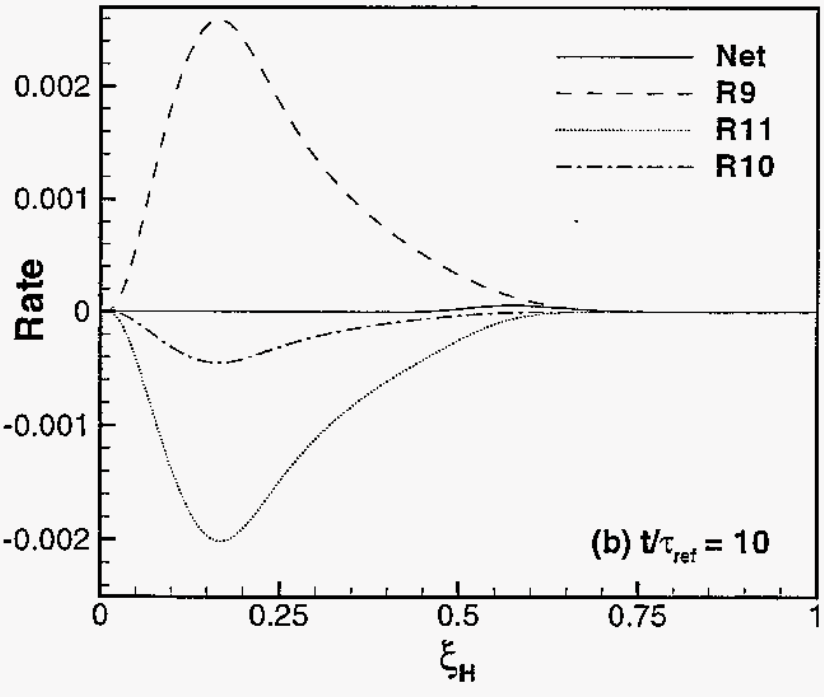

(b)

Figure 5: Contributions of individual elementary reaction steps to the net reaction rate of HO_2 for the one-dimensional problem; (a) $t/\tau_{ref} = 5$ and (b) $t/\tau_{ref} = 10$.

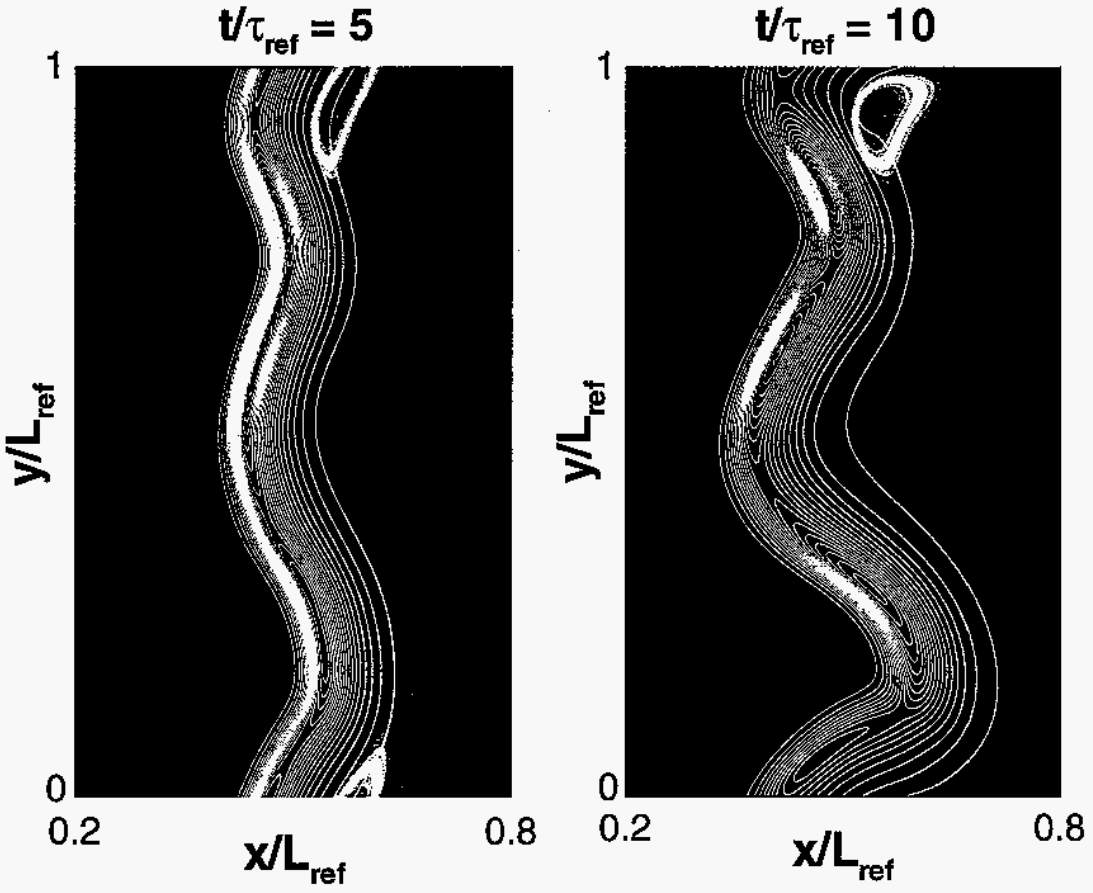

Figure 6: Contours of Y_{H} (color) and χ_{H} (line) at an earlier stage ($t/\tau_{ref} = 5$) and near ignition ($t/\tau_{ref} = 10$) for the weak turbulence case.

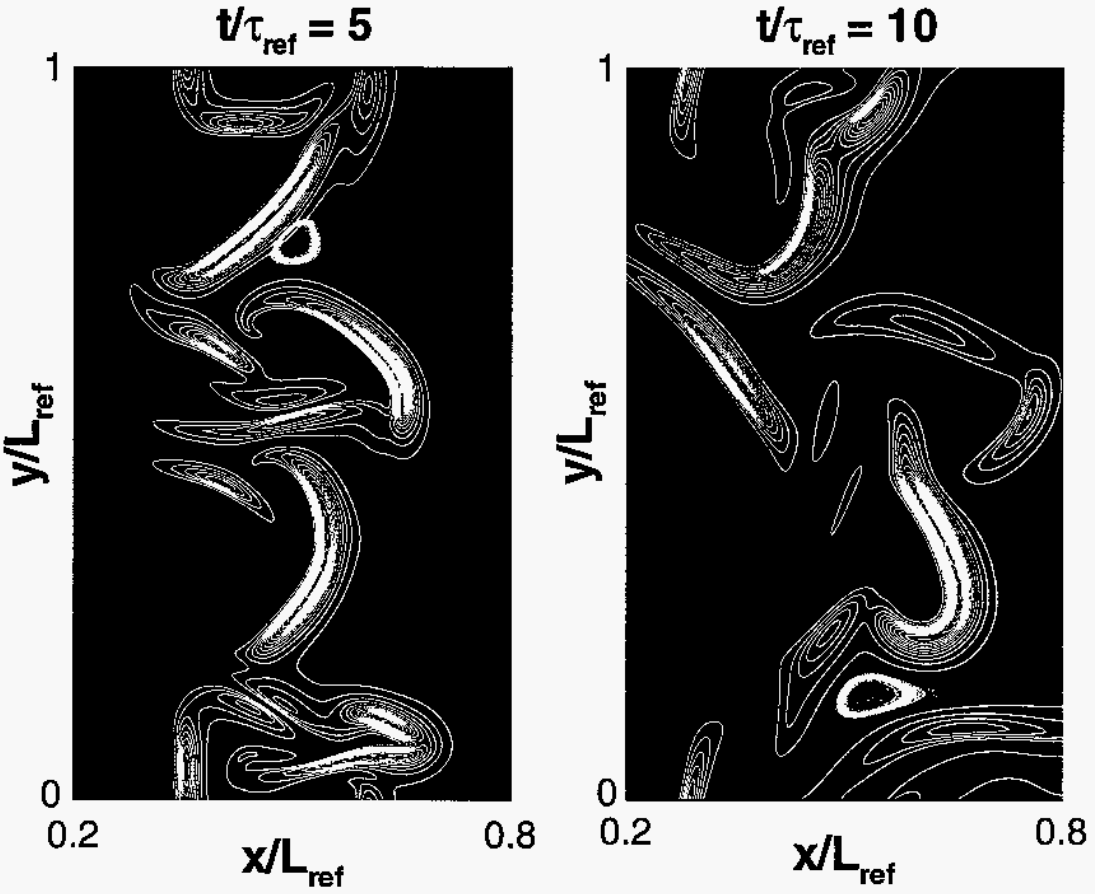

Figure 7: Contours of Y_H (color) and χ_H (line) at an earlier stage ($t/\tau_{ref} = 5$) and near ignition ($t/\tau_{ref} = 10$) for the strong turbulence case.

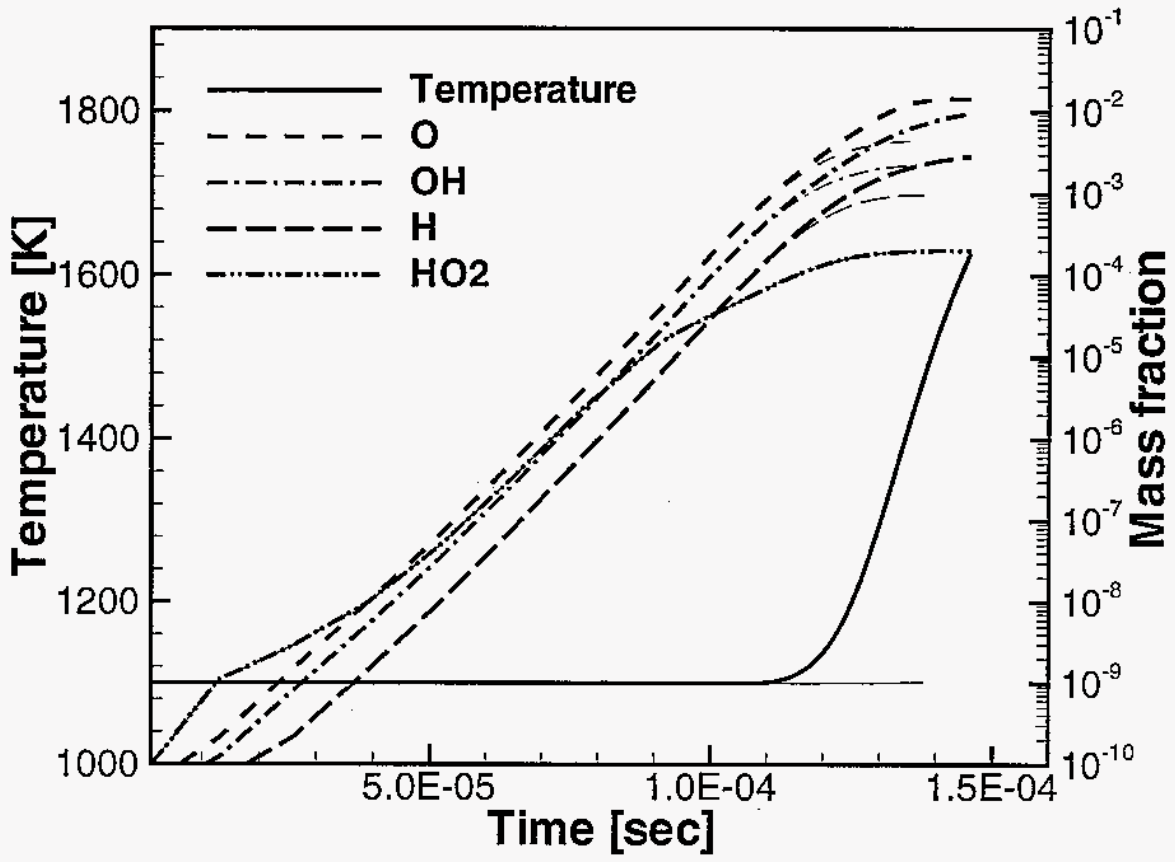

Figure 8: Maximum temperature and species as a function of time for weak turbulence case, $\tau_{turb}/\tau_{ig} = 3$; bold line denotes with heat release and thin line denotes without heat release.

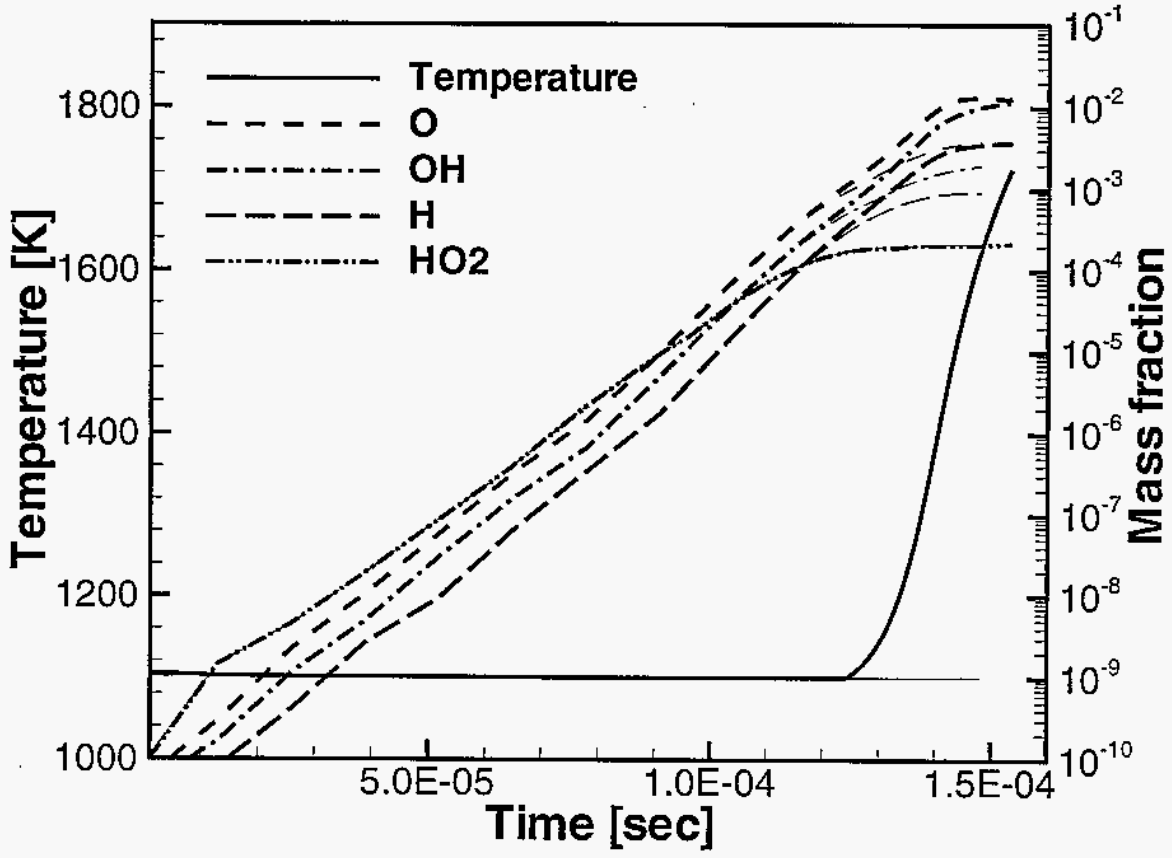

Figure 9: Maximum temperature and species as a function of time for strong turbulence case, $\tau_{turb}/\tau_{ig} = 0.3$; bold line denotes with heat release and thin line denotes without heat release.

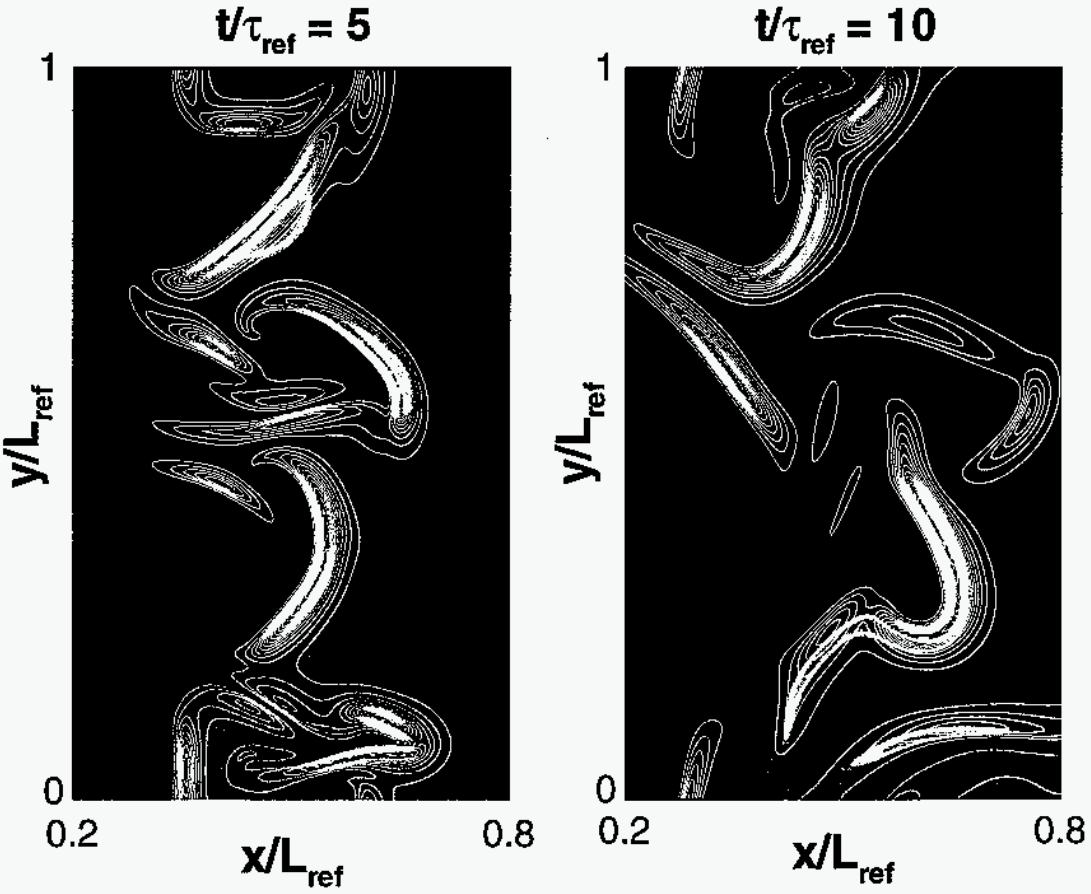

Figure 10: Contours of Y_{HO_2} (color) and χ_H (line) at an earlier stage ($t/\tau_{ref} = 5$) and near ignition ($t/\tau_{ref} = 10$) for the strong turbulence case.

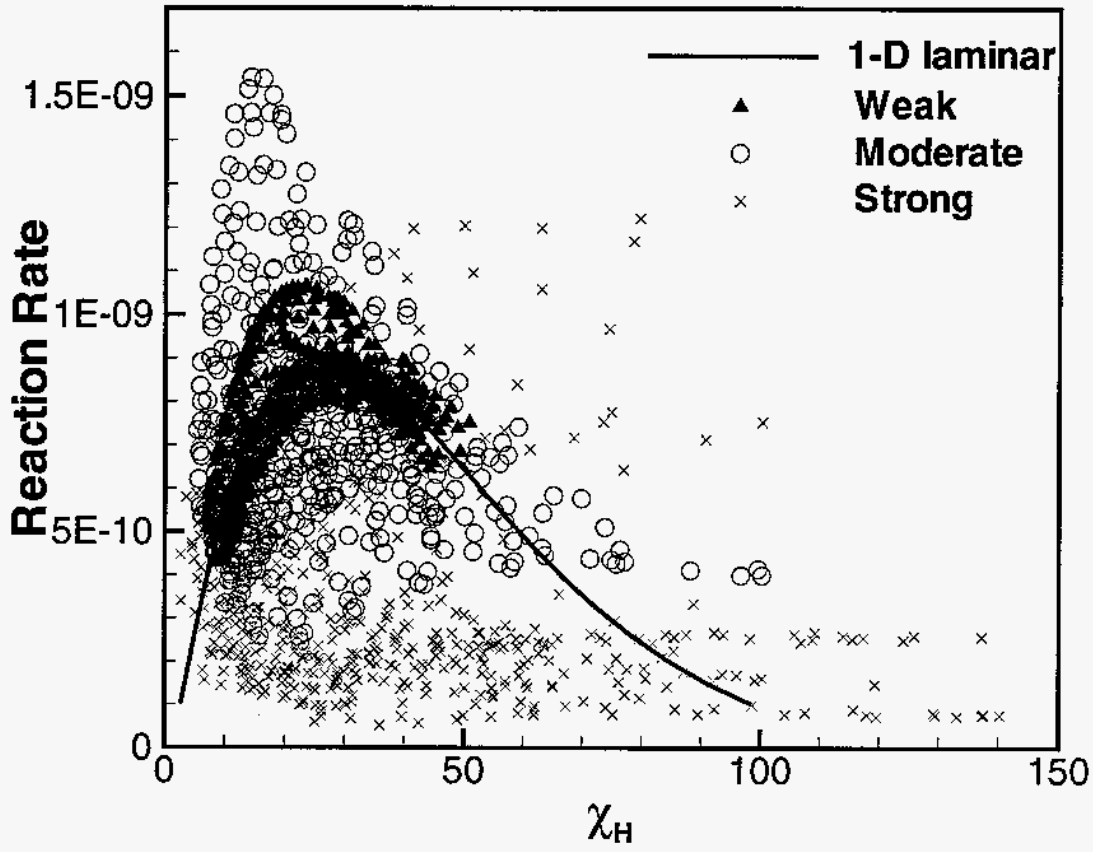

Figure 11: Scatter plot for the reaction rate of H as a function of scalar dissipation rate for three turbulence cases at $t/\tau_{ref} = 3$. Solid curve denotes the one-dimensional laminar result. The turbulent data are conditioned around $0.05 < \xi_H < 0.15$ for which maximum reaction rate is obtained.

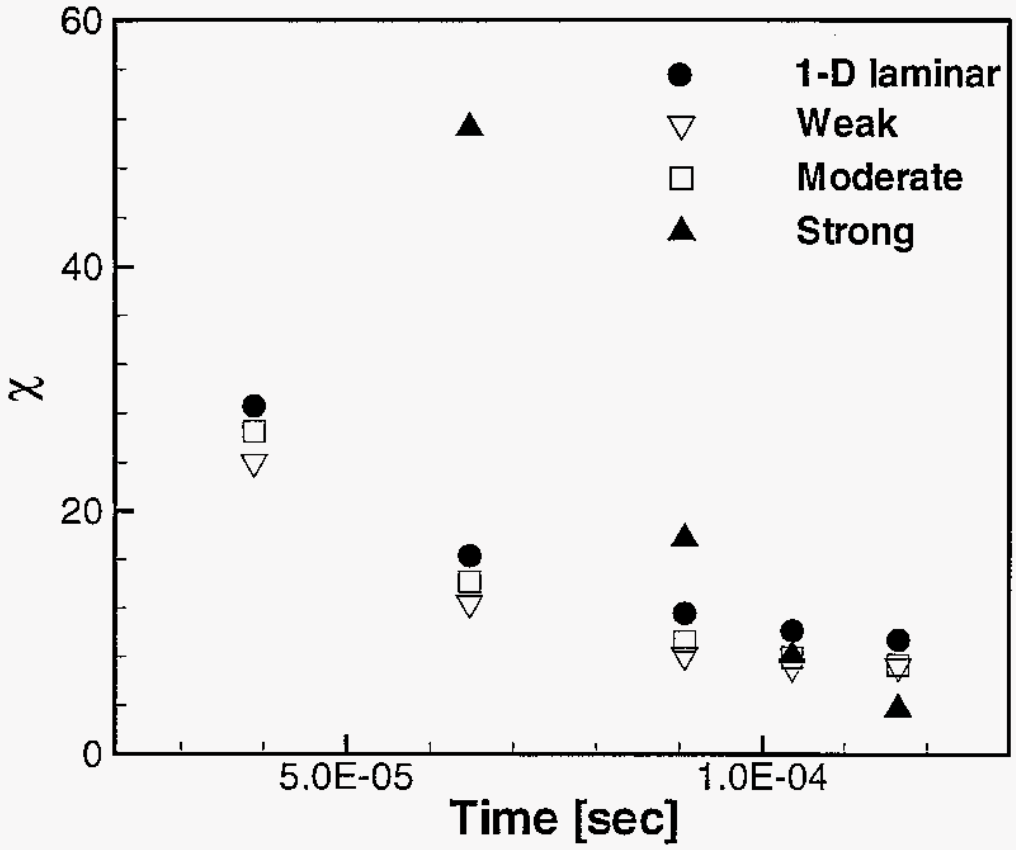

Figure 12: History of local scalar dissipation rate at the ignition kernel at which ignition finally occurs.

Report Number (14) SAND-98-8222C
CONF-980804

Publ. Date (11) 199808
Sponsor Code (18) DOE/LD, XF
UC Category (19) UC-1109, DOE/ER

DOE